ADC Noise Reduction and Characterization of a Compact Michelson Interferometer

Author:
Kristen ZYCH

Supervisors:
Dr. David RABELING
Prof. Dr. Jo van den BRAND

July 30, 2012

1   Introduction

The existence of gravitational waves was theorized early in the twentieth century by Albert Einstein in his theory of general relativity. Gravitational waves are "ripples" in space-time that come from high mass sources such as binary star systems or black holes. As a source moves, gravitational waves propagate outward and are thought to move at the speed of light and when they finally reach an observer, the disturbance can be sensed as the distance between free bodies expand and contract. Sensing this change in distance is the main goal of experiments such as Virgo and LIGO.[1] These collaborations built and operate huge Michelson interferometers (See Figure 1); these interferometers measure the relative motion between two essentially free body mirrors. The mirrors are held at right angles so that the passing gravitational wave will stretch one arm while it contracts the other. Moving the mirrors in this way will produce a detectable electromagnetic change in the output signal of the laser where the beams of the interferometer recombine and add constructively or destructively. Because gravitational waves interact weakly with matter, to date, a gravitational wave has yet to be directly detected.
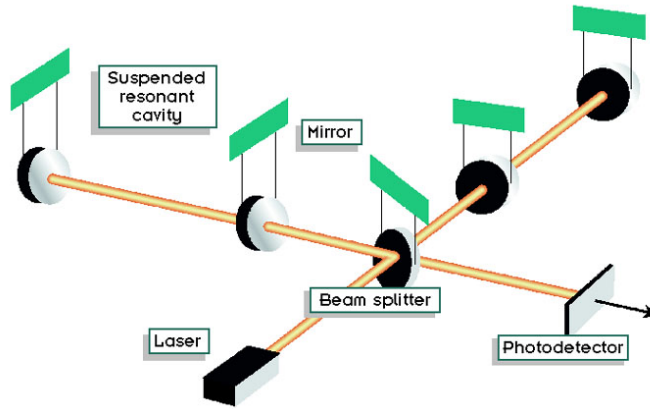

Figure 1: Laser interferometer schematic.[2]

In the ongoing search for gravitational waves, the Virgo collaboration deals heavily in noise attenuation techniques. Sources of seismic noise must be identified and mitigated because if they are not, the weakly interacting gravitational wave, which is expected to move the test mass only 10^{-19} meters, will be masked by other disturbances. Nikhef is a research facility in Amsterdam, the Netherlands, that is part of the Virgo collaboration. At Nikhef there is a project under development involving a multistage seismic attenuator system referred to as MultiSAS (Figure 2a). This experiment calls for a diagnostic device that will confirm the performance and sensitivity of the MultiSAS; commercial seismometers and geophones are not sensitive enough, therefore a horizontal inertial sensor is being worked on simultaneously.[3] This accelerometer needs a sensitivity on the order of femtometers and this can only be realized by minimizing various souces of noise such as measurement noise, ground noise, relative intensity noise, etc. The accelerometer is shown in Figure 2b, it consists of a folded pendulum and a compact interferometer on the right as the sensing device. This paper describes how measurement noise was decreased and also describes the characterization and evaluation of the interferometer.
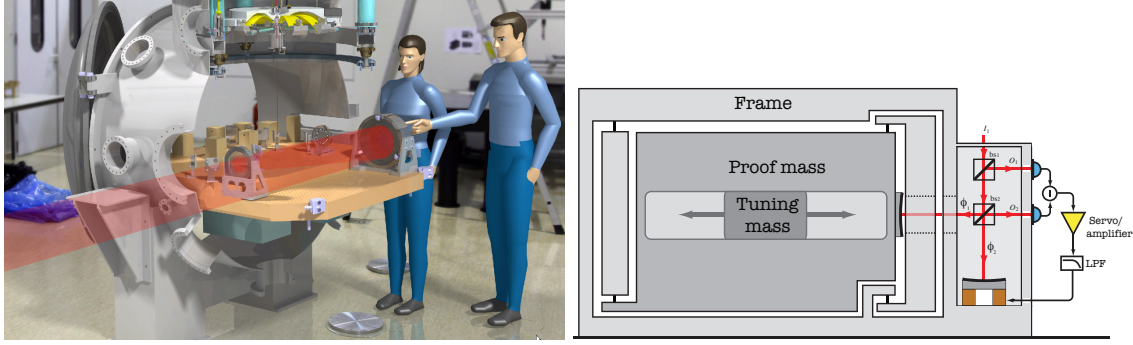
Figure 2: a) The MultiSAS under development at Nikhef. b) Accelerometer

2   Reducing ADC Noise

2.1   The ADC

ADC stands for analog-to-digital converter and is a device that samples a continuous signal thereby changing it into a digital, discrete form. The data acquisition device used was a NI-6289 ADC which utilized a 2090A BNC converter to interface with the ADC card. All ADCs have quantization error, or quantization noise, that results from digitizing the waveform signal. The digitization defines a voltage resolution due to a minimum resolvable voltage step. This step is given by the following equation[4]

$$\Delta = \frac{Vpp}{2^N},\tag{1}$$

where Vpp is the peak-to-peak input voltage setting and N is the number of ADC bits. Further, the actual quantization error is less than or equal to half this step size because of rounding. This is an 18-bit device that has a quantization error on the order of 10^{-5} V for a 20 Vpp input under typical operation. The best way to evaluate the dynamic range of the ADC is as a function of frequency[5] and here we will use amplitude spectral density,

$$ASD_{noise}(f) = \sqrt{\frac{\Delta^2}{12 \cdot f_N}},\tag{2}$$

where f_N is the Nyquist frequency. The following sections show the noise floor at a particular sampling frequency and how the quantization noise is reduced by oversampling the ADC by different amounts.

2.2   Oversampling

The oversampling and averaging technique is implemented by sampling at a rate that is much higher than the target frequency. The oversampling ratio OSR is defined as

$$OSR = \frac{f_{os}}{f_s},\tag{3}$$

where f_{os} is the oversampling frequency and f_s is two times the Nyquist frequency of the input signal. The oversampling ratio can be substituted for f_N in eq. (2) and becomes

$$ASD_{noise}(f) = \sqrt{\frac{\Delta^2}{12 \cdot OSR}}. \tag{4}$$

Substituting eq. (1) into eq. (4) so that it is in terms of N and solving for N yields

$$N = -\frac{1}{2}\frac{\log(OSR)}{\log(2)} - \frac{1}{2}\frac{\log(12 \cdot ASD_{noise})}{\log(2)} + \frac{\log(Vpp)}{\log(2)}. \tag{5}$$

This equation shows that N increases by $1/2$ when the oversampling ratio is doubled or gaining one bit of resolution requires oversampling by a factor of 4,

$$f_{os} = 4^w \cdot f_s, \tag{6}$$

where w is *additional* bits of resolution, f_s is the original sampling frequency requirement and f_{os} is the oversampled frequency[4]. These samples are then added together and divided by 4^w, averaging data in this way is often called *decimation*. A snapshot of the LabView subroutine that averages the data is depicted in Figure 3. This trial sought to investigate the maximum bit resolution, i.e. noise reduction, possible with the given equipment. To do this, the sampling rate f_s was held at 2^7 (128) Hz while f_{os} and w were systematically increased to the performance limits of our data acquisition system.
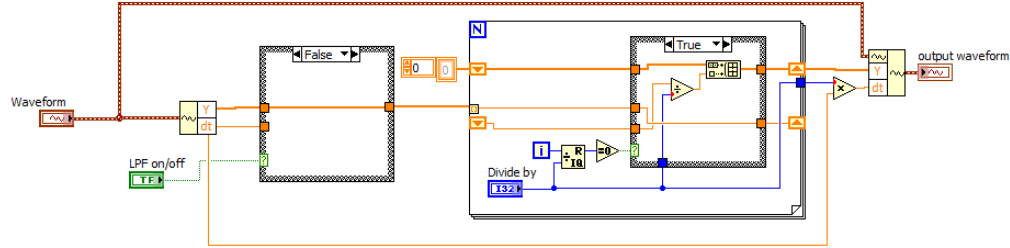

Figure 3: The conditional loop used to average the data.

2.3   System Limitations

There was a trade off between the largest bit resolution and the inherent increased noise that accompanies larger signals. The *effective number of bits*, N from eq. (5), can be calculated by recasting eq. (5) in a different form,

$$N = \frac{\log\sqrt{\frac{Vpp^2}{12 \cdot OSR \cdot ASD_{noise}}}}{\log(2)}. \tag{7}$$

Increasing the input voltage will increase the N but it also results in a higher noise floor which is not worth the ultimate gain in bits.
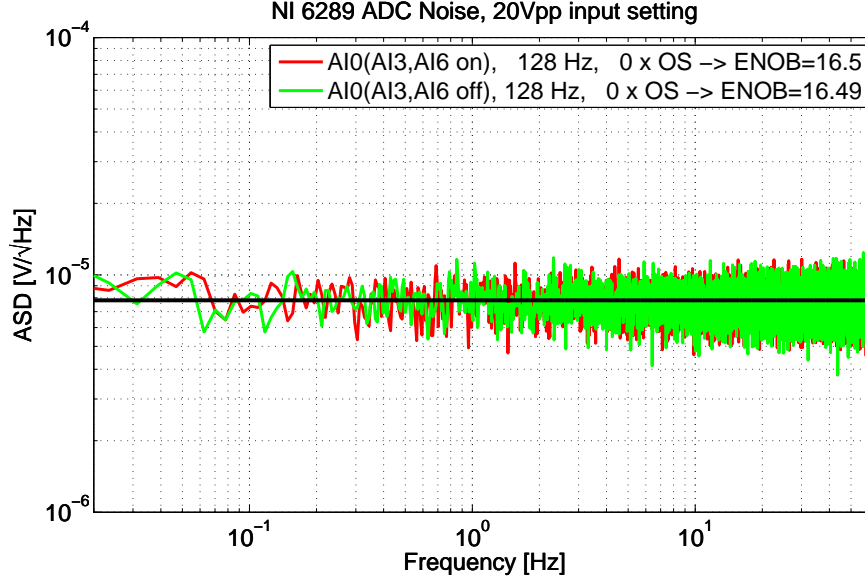
3

Figure 4: The noise is unaffected by increased channel usage.

It is desirable to get the maximum possible oversampling factor, but there exist certain limits with the equipment. Because the ADC does not sample from channels simultaneously, it must switch between channels, it was suspected that sampling from fewer channels at a time would decrease the noise. For example, the maximum sampling rate for the ADC is 500 kS/s. To sample from more than one input channel then the aggregate sampling rate over all channels must be less than or equal to 500 kS/s. As f_{os} increases fewer channels can be used; although interestingly, using more than one channel at a time does not increase the noise as evidenced by Figure 4.

There was also a computational limit when f_{os} transcended 100 kHz. The data throughput was too high for the computer to handle and the virtual memory could not sustain the calculation without data loss.

2.4 Results of Oversampling

It was possible to decrease the noise from 1×10^{-5} V/$\sqrt{Hz}$ to 6×10^{-7} V/$\sqrt{Hz}$ for 1 Hz and beyond with a 20 Vpp input setting. The lower frequency range from 10^{-2} to 1 Hz experiences a similar decrease in noise but is heavily influenced by $1/f$ noise, so the effect of oversampling is diminished. Figure 5 demonstrates the differences between initial input voltage settings. For a 2 Vpp input setting the ADC's noise floor starts at 10^{-6} and the effects of oversampling are only felt above 1 Hz, at the highest oversampling possible the signal never flattens out.

Figure 6a shows some of the sources of noise that accompany the accelerometer and are converted to displacement. To compare, Figure 6b shows how oversampling reduces the noise such that the signal will not dominate the accelerometer noise floor beyond 10 Hz. To conclude, it is possible to decrease the quantization noise of an ADC by between 1 and 2 orders of magnitude making a better

4

SNR without resorting to more costly devices simply by oversampling data. Lastly, this process allows us to meet the required noise floor which is a step closer to reaching accelerometer's desired sensitivity of 10^{-15} meters.
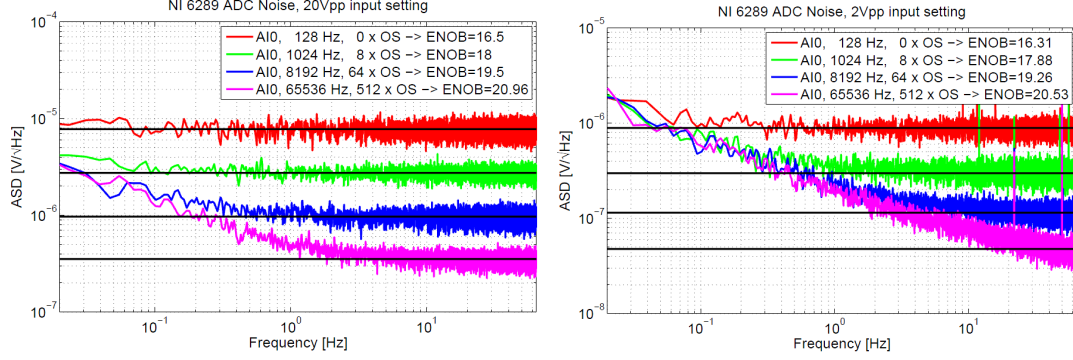

Figure 5: The oversampling factor increases by a factor of 8 and the bit resolution is increased with each step.
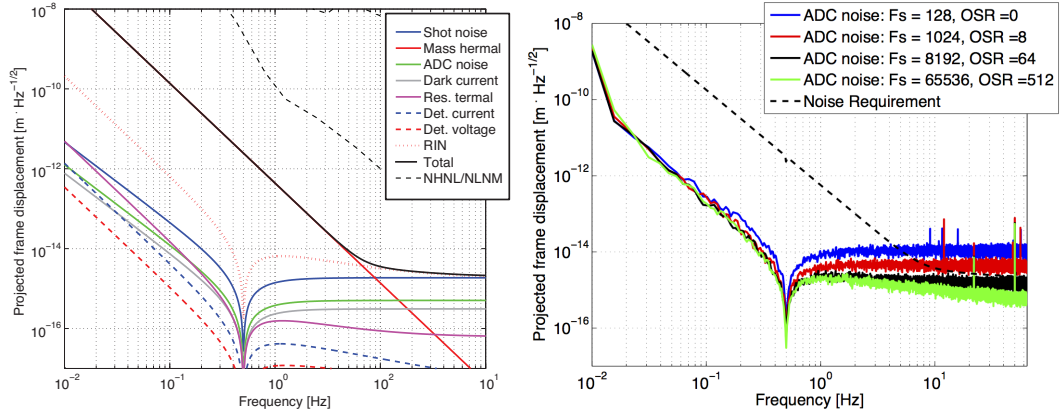

Figure 6: a) Component-wise noise budget for accelerometer.[6] b) Without oversampling, signal beyond 10Hz is dominated by ADC quantization noise
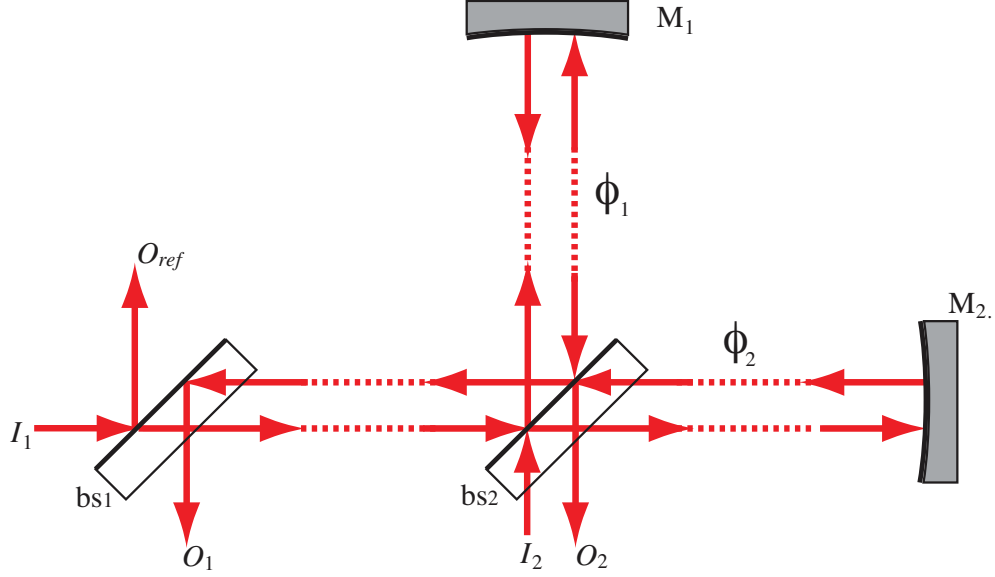
Figure 7: A Michelson interferometer schematic. I_1 is the input light and O_1 and O_2 are the recollected outputs. ϕ_1 and ϕ_2 are the round trip phase differences.[6]

3 Michelson Interferometry

From a Michelson interferometer, we can calculate the round trip phases and outputs; Figure 7 shows the components of the interferometer's path. If L is the common arm length or the distance from the second beamsplitter (bs2) to the mirrors, M_1 and M_2, and z is the difference between the arm lengths, then,

$$\phi_1 = 2\frac{\omega_c L}{c} \tag{8}$$

$$\phi_2 = 2\frac{\omega_c (L + z)}{c} \tag{9}$$

where ω_c is the frequency of the laser in rad/s and c is the speed of light. ϕ_1 and ϕ_2 are indicated in Figure 7. The outputs from the interferometer are the following,

$$O_1 = I_1 i t_{bs1} r_{bs1}\left(r_{bs2}^2 \exp[i\phi_1] - t_{bs2}^2 \exp[i\phi_2] \right) \tag{10}$$

$$O_2 = -I_1 t_{bs1} r_{bs1}\left(t_{bs2} r_{bs2} \exp[i\phi_1] + t_{bs2} r_{bs2} \exp[i\phi_2] \right) \tag{11}$$

where $t_{bs1,2}$ and $r_{bs1,2}$ are the transmission power and reflection power coefficients and are taken to be 50%.

The outputs from the system can then be used to define what the transfer function equations for reflection and transmission are, $\mathcal{R}$ and $\mathcal{T}$ respectively.

$$\mathcal{R} = \frac{O_1}{I_1} = \frac{1}{\sqrt{2}}\left(\frac{\exp[i2\omega_c L/c]}{2} - \frac{\exp[i2\omega_c(L+z)/c]}{2}\right)$$

$$= \frac{i}{\sqrt{2}}\sin(\omega_c z/c)e^{(2i\omega_c L/c)} \tag{12}$$

$$\mathcal{T} = \frac{O_2}{I_1} = -\frac{1}{2}\left(\frac{\exp[i2\omega_c L/c]}{2} + \frac{\exp[i2\omega_c(L+z)/c]}{2}\right)$$

$$= -\frac{1}{2}\cos(\omega_c z/c)e^{(2i\omega_c L/c)} \tag{13}$$

And then we have the reflected and transmitted power using the absolute square of the above equations, $|\mathcal{R}|^2$ and $|\mathcal{T}|^2$,

$$P_{\mathcal{T}} = P_{inc}\left[\frac{1}{4} + \frac{\cos(2\omega_c z/c)}{4}\right] \tag{14}$$

$$P_{\mathcal{R}} = P_{inc}\left[\frac{1}{8} - \frac{\cos(2\omega_c z/c)}{8}\right]. \tag{15}$$

3.1 Experimental Setup

The interferometer design used in this experiment is a semi-monolithic Michelson interferometer that has an LED as a light source. The device is semi-monolithic because it has four metal pieces that are held together with screws. The arms lengths are approximately 1.5 cm and one of the mirrors is mounted on an aluminium wall that is perpendicular to a second mirror that is glued to a piezoelectric disk. Two beam splitters guide the light and two photodiodes collect it and feed the converted signal out to the servo. The servo is part of the control system which is discussed in the following section.

With an interest in low cost and a compact design, an LED was chosen for a light source. It was mounted in the wall of the interferometer opposite from the piezoelectric actuator and shone through a pinhole to collimate the light. In the time that is paper was written, it was not possible to find the correct distance that this wall had to be positioned in order to see interference fringes. This was because the coherence length for an LED source is short (about 10μm)[7] with a tolerance for seeing fringes of approximately ± 5 microns and it proved difficult to accurately dial in the arm lengths. Beyond the arm lengths, making sure the beams were aligned was also challenging because it is possible that the mirrors were not sitting flat (the two were epoxied in place) or that the walls could not be screwed together at a truly right angle, or further, that the beam splitters were not in the right location and orientation. For this reason, the wall holding the LED was removed and a helium-neon laser, which has a coherence length on the order of 1 meter,[8] was substituted so that the system could be characterized.

3.2 Control Theory

In order to characterize the system, the interferometer must be held in lock. Control loops are used to keep a parameter of choice in a stationary or close to stationary state. These loops are composed of two basic parts: there is the plant and a servo, see Figure 9.[9] The plant is the system under investigation, it employs the chosen parameter, and it has two important subsystems: namely, the
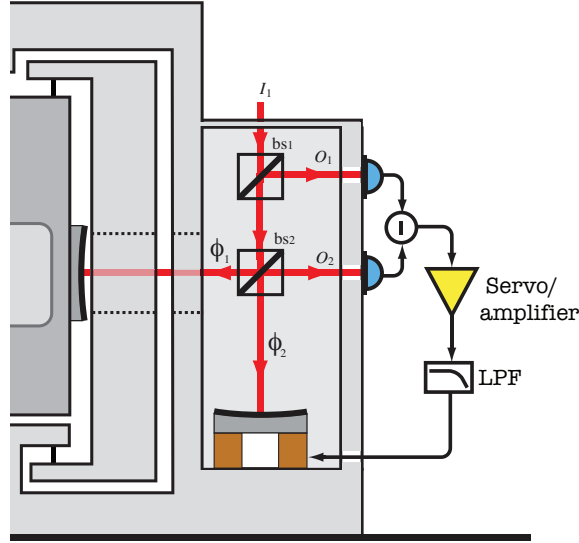
Figure 8: Interferometer attached to inverted pendulum of accelerometer. [6]

sensor and actuator. The sensor is what measures the controlled parameter, or more precisely, it measures the fluctuation from some set point. The actuator is the part of the loop that corrects this deviation, it can be a piezoelectric material or a valve, etc. For example, if the controlled parameter is voltage, the sensor senses any present deviation which is then fed to the servo, the servo acts accordingly, transforming the signal into a feedback signal that will correct the deviation. That signal is then fed to the actuator, the voltage is corrected, and the process begins again.
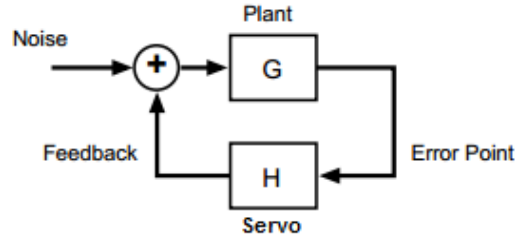

Figure 9: Simple feedback loop, all parts are in series. [9]

3.3 Open and Closed Loops

Probing and characterizing the system is achieved by taking its transfer function. A transfer function is the complex ratio of the output signal to the input signal. The complex values hold both magnitude and phase information and are a function of frequency. It is simple to calculate the transfer function, which is also known as gain, for an open loop system whose components are

either in series or in parallel. For components that are in series, the total gain is just the complex product of the gains. Meanwhile, for components that are in parallel, the total gain is the complex sum of the individual gains.[9]

In series:

$$G(f) = G_1 \times G_2 \tag{16}$$

In parallel:

$$G(f) = G_1 + G_2 \tag{17}$$

And these equation are used upon closing the loop when calculating the gain for the individual parts and for the whole setup. Figure 11 shows how the gain from the interferometer is acquired. A signal is fed in to the piezo, the signal is detected by the photo detector, and that is converted into some output voltage. For this interferometer the gain is about 1/32 [V/V].

Figure 9 shows how a noise signal (or a signal from something more interesting) and a feedback signal are combined into signal s and fed into the plant.

$$s = Noise + Feedback \tag{18}$$

Then that signal is acted on by the plant and the servo which is then turned into feedback.

$$Feedback = s \times G \times H \tag{19}$$

where G and H are in reference to Figure 9 for the plant and the servo, respectively. By manipulating these equations you can find the gain, the ratio of the input to the output, of the closed loop and it is denoted this way

$$Gain = \frac{1}{1 - (G \times H)} \tag{20}$$

and this also represents the transfer function of the loop. The interferometer is held is lock when the loop is stable. A stable loop is held at the operating point and does not oscillate around that point.

3.4   PID Controller and Locking the Interferometer

The main way to evaluate the loop, which consists of an interferometer, photodetector, an high voltage amplifier, a low pass filter, and a PID controller (called a Lockbox) is to take its transfer function. While using the HeNe laser, the interferometer was locked halfway up a fringe. By locking the interferometer we ensured that the relative difference in optical path lengths between each of the arms stayed constant. To do this we subtracted a voltage from the transmitted Michelson fringe, such that the signal became zero crossing on the linear part of the sine wave. This could now function as our correction signal. Any deviation from the zero point would tell us whether a deviation had taken place, plus the sign of the error would give the direction of the deviation. The right part of Figure 11 shows where the interferometer is locked on the linear part of a sine wave. This set up uses negative feed back and if it finds itself trying to lock on the section of linearity with a positive slope, it is automatically pushed beyond that to where it can find the negative slope again. In order to acquire the transfer functions of the system, a premade LabView frequency response function (FRF) program was used. The idea behind this program is that it feeds a stimulus signal into the loop and also into the input of the data acquisition device. The
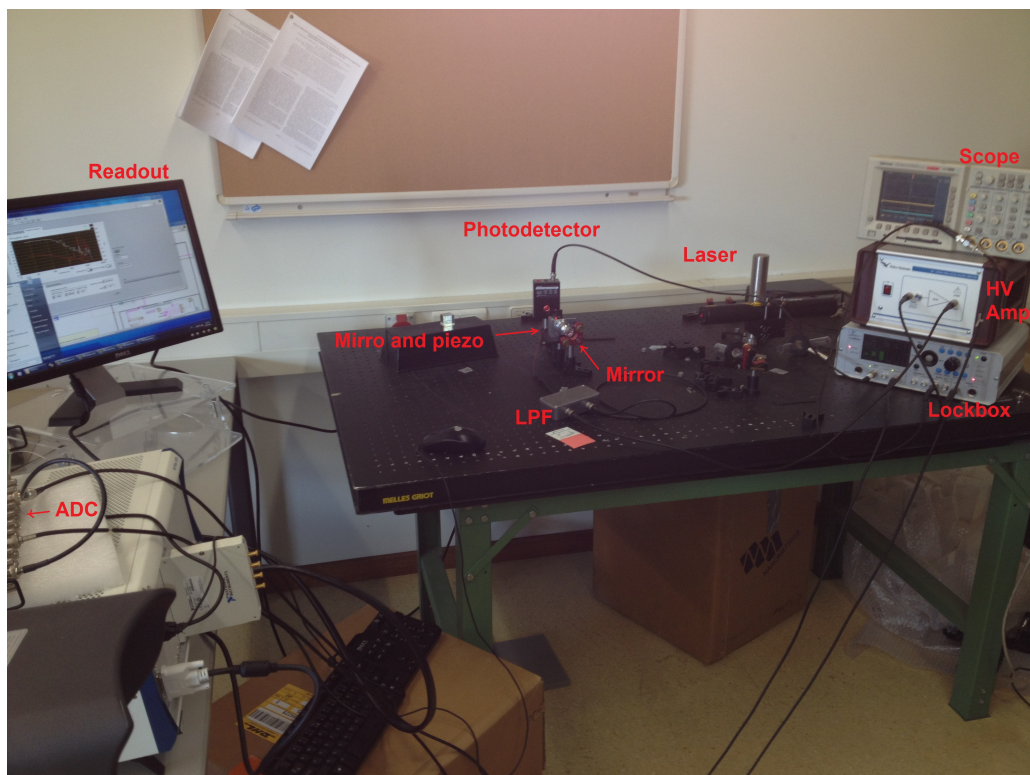
9

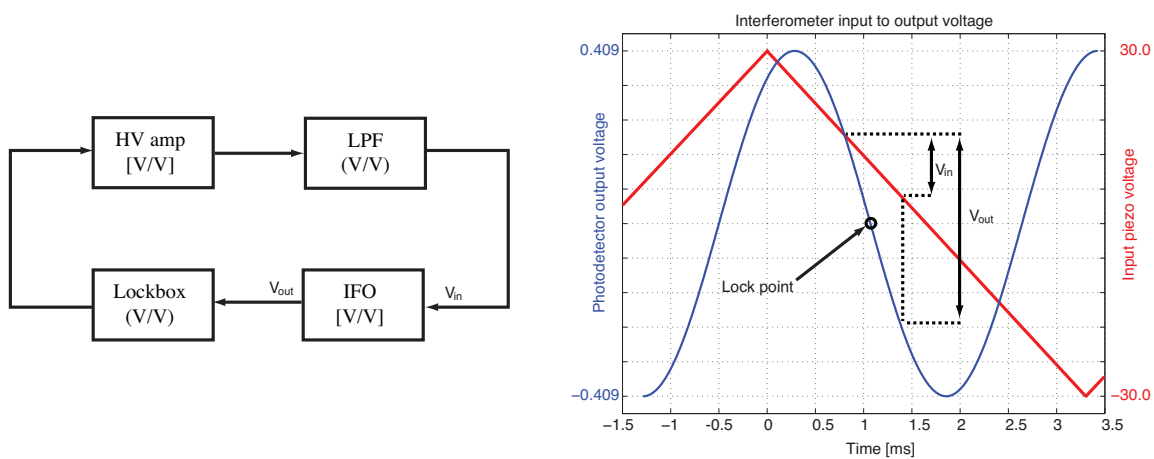Figure 10: Interferometer set up used for characterizing the system.

Figure 11: Fringe locking.

signal goes through the loop (the "device under test") and the FRF trace, which is the transfer function, is made by taking the quotient of the signal that goes through the device to the stimulus signal.
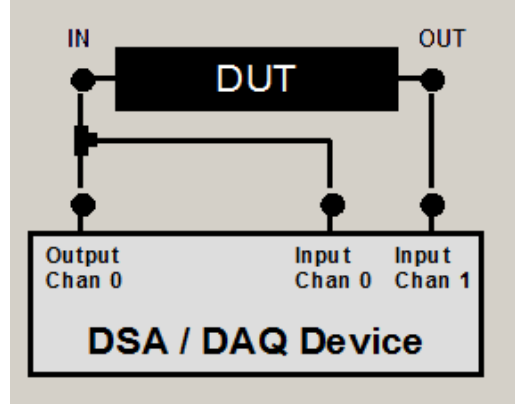

Figure 12: Setup for the transfer function measurements.

3.5   Results

Figure 14 shows the predicted closed loop transfer function of the system with various gains coming from the Lockbox. Figure 14 and 15 that show the modeled and the experimental closed loop transfer functions of the whole system. It is important to point out that the 3dB bandwidth that was predicted is approximately 1.7 kHz while the experimental 3dB bandwidth is around 1.6 kHz. These plots also show how increasing the gain from the Lockbox increases the bandwidth of the system. In the experimental closed loop transfer function, structural resonances are visible in the region beyond 3 kHz. These are the results that were expected from an interferometer of this type and for the devices that were used.
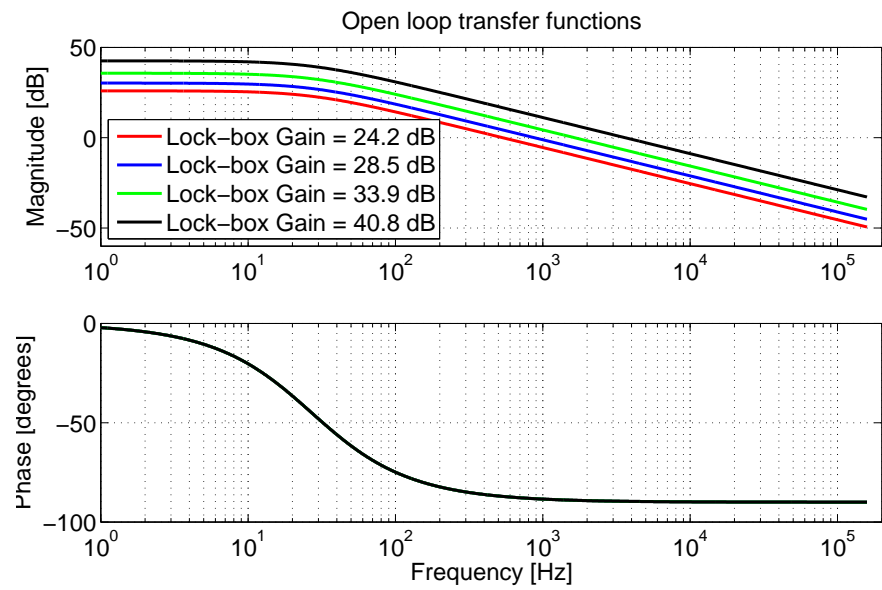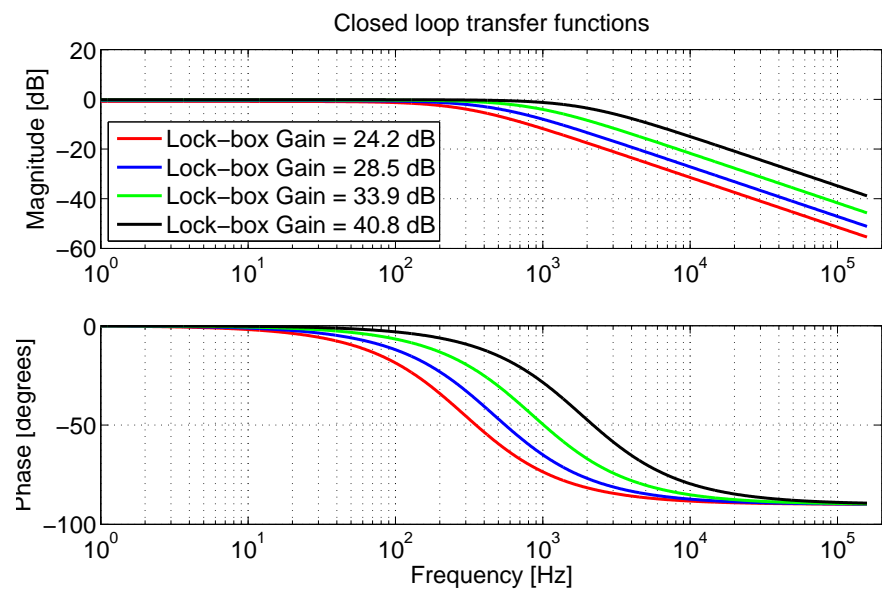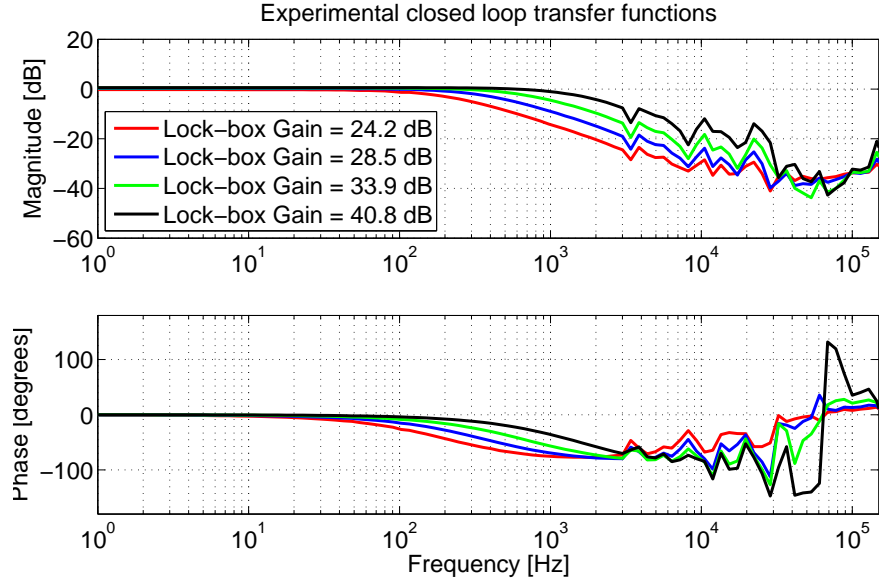
Figure 13

Figure 14

12

Figure 15

3.6 Conclusion

To conclude, implementing the ADC noise reduction for the data acquisition and readout system will bring the accelerometer one step closer to reaching its desired sensitivity of 10^{-15} meters at and above 10 Hz. The next step in this project will be to get the LED implemented and working properly in the interferometer so that it is possible to find fringing. An investigation of LED's relative intensity noise (RIN) must also be performed. Once this is achieved, the interferometer can be mounted on the accelerometer and from there system tests will be made and it will be closer to its purpose as a diagnostic tool for the MultiSAS.
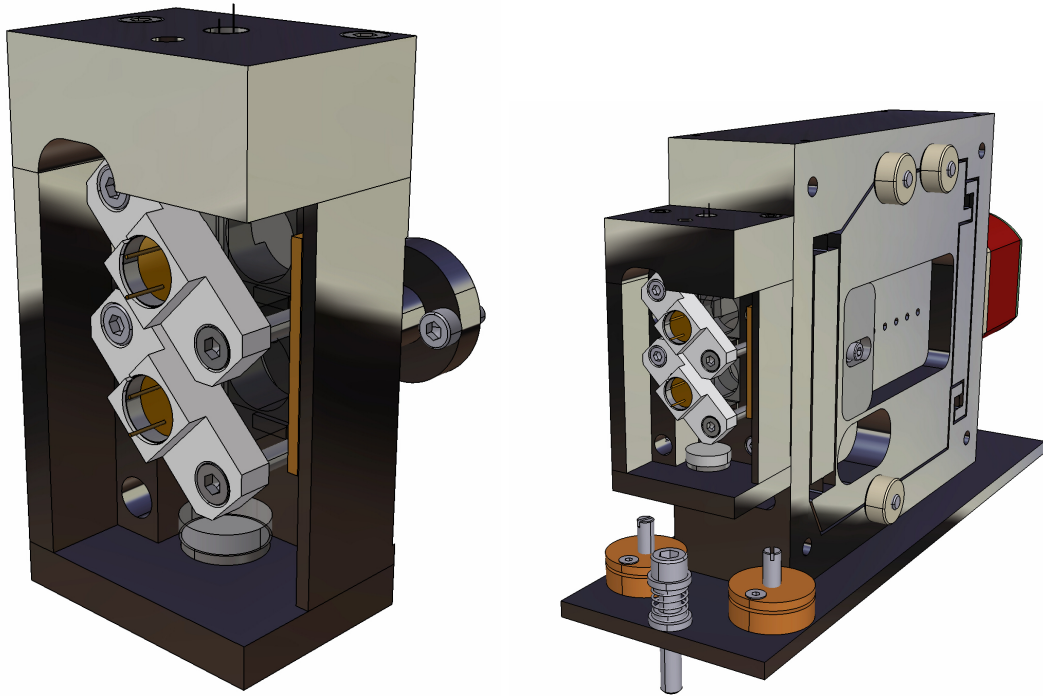
3.7 Acknowledgements

Figure 16

References

[1] Scott Hughes. *Listening to the Universe with Gravitational-Wave Astronomy.* Annals of Physics, February 2008.

[2] B. Abbott, *et. al., Detector description and performance for the first coincidence observations between LIGO and GEO.* Elsevier Vol. 517, Issue 1-3, pp. 154-179, January, 2004.

[3] Alessandro Bertolini, Riccardo DeSalvo, Francesco Fidecaro, Mario Francesconi. *Mechanical design of a single-axis monolithic accelerometer for advanced seismic attenuation systems.* November 28, 2005.

[4] *Improving ADC Resolution By Oversampling and Averaging*, CYGNAL Integrated Products, Inc. May 2001.

[5] Reinoud Sleeman, Arie van Wettum, and Jeannot Trampert. *Three Channel Correlation Analysis: A New Technique to Measure Instrumental Noise of Digitizers and Seismic Sensors.* Bulletin of the Seismological Society of America, Vol. 96, No. 1, pp. 258-271, February, 2006.

[6] Mark Beker, Jo van den Brand, Thomas Bauer, Eric Hennes, Alessandro Bertolini, Fred Schimmel, David S. Rabeling. *Nikhef Technical Note: System Requirements for Broadband Pico-g Seismometer Readout.* January, 2012.

[7] Malcolm Gray, David McClelland, Mark Barton, Seiji Kawamura. *A simple high-sensitivity interferometer position sensor for test mass control on an advanced LIGO interferometer.* Optical and Quantum Electronics 31: 571-582, 1990.

[8] Thorlabs.com HeNe Lasers: Red Thorlabs.com (2012) Thorlabs.com HeNe Lasers: Red. online Available at: `http://www.thorlabs.com/newgrouppage9.cfm?objectgroup_id=1516` [Accessed: 20 Jul 2012].

[9] Andreas Freise. *The Next Generation of Interferometry: Multi-Frequency Optical Modelling, Control Concepts and Implementation* Appendix B Control loops. 2003.

[10] Seiji Kawamura, Osamu Miyakawa, Shihori Sakata. "Calibration of the 40m Fabry-Perot Michelson Interferometer." Technical note, December, 2003.

[11] John Bechhoefer. *Feedback for physicists: A tutorial essay on control.* Reviews of Modern Physics, 77, 2004.